Journal of Hydraulic Structures
J. Hydraul. Struct., 2025; 11(3): 46-60
DOI: 10.22055/jhs.2024.47885.1321

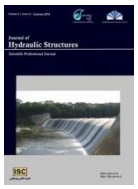

OPEN ACCESS

Numerical investigation of the effect of periodic turbulence promoters on the performance enhancement of nanofiltration modules

Mojtaba Azizi[*1]
Meysam Naderi[2]

Abstract

A new method for increasing the permeate flux of a nanofiltration module is presented. In a wall-patterned flat sheet membrane module, three distinct patterned walls were designed for the feed channel. 2D CFD modeling and simulation of the system's performance in nanofiltration of an aqueous solution of $MgSO_4$ were used to examine the impact of the turbulence promoters on the system's performance. The model's output was compared to the published experimental data; strong agreements were found. With varying feed flow rates, the largest variance for the permeate flux was 1.8%. The simulation results at different feed flow rates showed that applying geometric patterns on the opposite wall of the membrane in the nanofiltration module can enhance the permeate flux. The sine-wave pattern with a maximum increase of 48% of the permeate flux had the best performance among the investigated geometries under the same conditions. Response surface methodology (RSM) was used to investigate the impact of various operating parameters on permeate flux in a nanofiltration module with a Sine-wave patterned channel. RSM results showed that raising the transmembrane pressure (TMP) or the feed flow rate resulted in a noticeable improvement in the permeate flux. However, when the concentration of the feed was increased, the permeate flux tended to decrease.

Keywords: concentration polarization; CFD simulation; nanofiltration; water desalination.

Received: 29 August 2024; Accepted: 12 December 2024

1. Introduction

Many membrane techniques for treating salty water have surfaced in recent decades. The supply of drinking water can be improved with the development of membrane technology. The properties of semipermeable membranes are largely responsible for the separation in this method.

[*]E-mail: azizi.m_58@yahoo.com **(Corresponding author)**
[1] Faculty of Chemistry and Chemical Engineering, Malek Ashtar University of Technology, P.O. Box 16765-3454, Tehran, Iran.
[2] Department of Chemical Engineering, Amirkabir University of Technology (Tehran Polytechnic), Tehran, Iran.

Fouling, which may be categorized into several categories such as organic, colloidal, inorganic, and microbiological fouling, is the accumulation of particles in the feed channel. Concentration polarization (CP) events and membrane fouling may be the cause of the flux decline [1–3]. According to scientific evidence, the CP caused a 30% reduction in membrane performance [4]. Two methods of controlling the CP that have been proposed include lowering the water flux (J) and raising the mass transfer coefficient (K). Previous studies have demonstrated that the CP may be efficiently disturbed by increasing the liquid cross-flow velocity, adjusting hydrodynamic properties, and creating turbulent flow [5].

The last several years have seen a significant amount of experimental and computational study devoted to the CP phenomena. Through simulations using computational fluid dynamics (CFD), the study on turbulent promoters was established. As a result, it was evident that the turbulence promoters had an impact on a number of metrics, including the permeate flux, wall shear stress, mass transfer boundary layer, and so on. Subramani et al. [6] used finite element modeling to study the behavior of pressure, flow, and concentration profiles in open and spacer-filled membrane channels for reverse osmosis (RO) and nanofiltration (NF) systems. In their study, open channels were compared to various spacer-filled configurations (cavity, submerged, and zigzag) to evaluate the impact on pressure drop and concentration polarization. Results indicated that pressure drops were 2–5 times higher in spacer-filled channels, with the submerged spacer exhibiting the highest drop. Additionally, CP was generally reduced in spacer-filled channels, particularly with the cavity spacer, which showed lower CP than both open channels and other spacer types. These findings suggest that cavity spacers may offer optimal performance for minimizing CP while balancing pressure losses.

Ahmad and Lau [7] employed CFD simulations to examine the effects of different spacer filament geometries on unsteady hydrodynamics and concentration polarization in spiral wound membrane channels. In their study, cylindrical, rectangular, and triangular spacers were compared, resulting in distinct effects on flow characteristics and polarization. Specifically, cylindrical spacers generated lower concentration factors (by up to 20%) at low Reynolds numbers (below 400) compared to rectangular spacers, highlighting their suitability as feed spacers. The transition to unsteady flow was shown to emerge at Reynolds numbers as low as 200 for cylindrical and triangular spacers, whereas rectangular spacers required Reynolds numbers above 300 to achieve similar unsteady flow effects.

Sreedhar et al. [8] employed 3D printing to develop triply periodic minimal surface (TPMS)-based feed spacers for enhancing flux and reducing biofouling in reverse osmosis and ultrafiltration (UF). In their study, TPMS-based spacers (Gyroid-sk, CLP-sh, and Schwarz P-sk) were compared to a commercial feed spacer, leading to 38% and 15.5% flux improvements in UF and RO, respectively, and a 92% reduction in bacterial cell adhesion with the Gyroid-sk spacer. The feed channel pressure drop also decreased by up to 12.5% compared to the commercial spacer, highlighting the TPMS spacers' efficiency in maintaining flow while mitigating fouling and pressure issues.

Abbasi Monfared et al. [9] used CFD to simulate various baffle arrangements aimed at enhancing permeate flux in gelatin-water ultrafiltration. In this study, six baffle configurations were analyzed in a rectangular channel, comparing them to a simple, unbaffled channel. Results indicated that the most effective central baffle arrangement achieved up to an 18% increase in permeate flux, raising it from 4.09×10^{-3} m^3/m^2s to 4.83×10^{-3} m^3/m^2s, while also showing higher values in turbulent kinetic energy and dissipation rate compared to other configurations.

Asefi et al. [10] employed 2D CFD simulation to simulate concentration polarization in a nanofiltration membrane module. The researchers investigated the impact of feed flow and

transmembrane pressure (TMP) on the rate of permeate flux and concentration. The effects of these differences were captured using a statistical technique called Response Surface Methodology (RSM). The results indicated that elevating the TMP or flow rate had a positive impact on the permeate flux, however increasing the feed concentration had a negative effect on it. The simulated results were verified by comparing them to experimental data, and they showed a high level of agreement. The mass transfer coefficient was also examined between CFD simulations and empirical correlations.

Fadhila et al. [11] employed Direct Numerical Simulation (DNS) using OpenFOAM to analyze oscillating inlet conditions within a membrane channel, aiming to enhance flow dynamics and reduce fouling in reverse osmosis systems. They compared oscillating inlet conditions (sine-wave and square-wave pulses at 1, 4, and 8 Hz) to a steady inlet flow, with simulations at a Reynolds number of 350. Results indicated that oscillating flows reduced low-shear zones by 40-50%, promoting flow instabilities that minimized stagnation regions, in contrast to steady flows, which generated larger recirculation regions and increased stagnation near spacer elements.

Dun et al. [12] investigated the effects of micro- and nanobubbles on fouling control and cleaning efficiency in nanofiltration membranes used for high-hardness water treatment. In their study, continuous and intermittent introduction of micro/nanobubbles was compared to using scale inhibitors, with continuous micro/nanobubbles resulting in a 6.3% higher membrane flux compared to the control group without scale inhibition. Over four cleaning cycles, flux reduction was lowest for pickling (22%), followed by alkaline washing (25%), and was highest with micro/nanobubble cleaning (33%). Despite a slightly lower cleaning efficiency, micro/nanobubbles minimized membrane aging without altering surface properties, offering an eco-friendly cleaning alternative.

Shang et al. [13] utilized a CFD model validated with Laser-Induced Fluorescence (LIF) to study concentration polarization suppression in nanofiltration. In their study, patterned membranes (triangular and cambered) were compared to a flat membrane surface, resulting in up to 13% reduction in maximum local concentration near the membrane surface for the cambered pattern. Additionally, the CP layer thickness on patterned surfaces decreased from 80 μm to 20 μm compared to the flat membrane. The local mass transfer coefficient on cambered surfaces was observed to be 3 times higher than on flat surfaces, while the CP factor reduced from 0.31 on flat surfaces to 0.15 on cambered surfaces.

Based on the literature review, increasing the flow turbulence on the membrane surface to reduce concentration polarization is an effective way to increase the permeate flux and reduce the membrane fouling. Increase of flow rate, oscillating flow, air bubbling, membrane surface patterning, use of spacers, and inserting baffle in feed channel are the most introduced methods for reducing the membrane polarizations and fouling. Among the mentioned methods, the application of baffles is the easiest and cheapest way to increase the flow turbulence on the membrane surface without any side effects on the membrane or operation. The application of baffles in the feed channel instead of feed spacers has the benefit of eliminating the dead areas on the membrane surface caused by the contact of the feed spacer and membrane surface. This work utilizes a CFD model that includes transport phenomena to enhance the water flux magnitude in various patterns applied to the feed channel shape to enhance turbulence intensity.

2. Materials and Methods

This work introduces a comprehensive two-dimensional computational fluid dynamics model that was created to examine the movement of water in a water desalination process utilizing a flat sheet nanofiltration technology. The model addresses two transport phenomena: mass transport

and momentum transport towards the feed channel. The feed in this model consisted of an aqueous solution of $MgSO_4$.

2.1. Geometry Design

Three unique designs and one conventional channel with a commercial feed spacer were created using the COMSOL Multiphysics 6.1 program. To ensure an equitable assessment of the effect of each pattern on the membrane flux, all patterns were deliberately designed to have the same periodic lengths (2.78mm). The length mentioned is equivalent to the gap between the filaments of a commercially available spacer, as described in reference [10]. These patterns may reduce concentration polarization and enhance permeate flux by promoting mixing in the feed channel and disrupting the concentration boundary layer.

Figure 1 displays the shapes and dimensions of the investigated channel with geometric patterns, which include prism, groove, and sine-wave patterns.

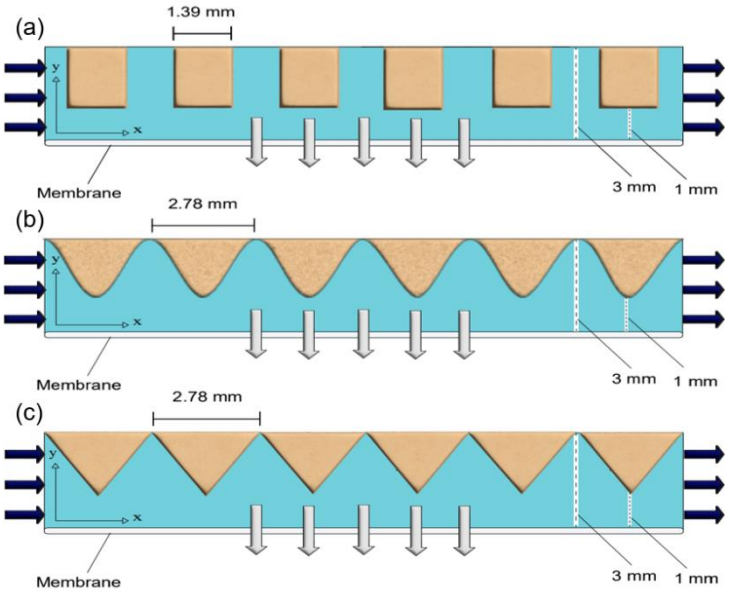

Figure 1. side view of a feed channel with several patterns on the upper wall: a) groove pattern, b) sine-wave pattern, c) prism pattern.

2.2. Governing Equations

The study employed the Analytical film theory paradigm to streamline an intricate transportation issue. This theory neglected the axial mobility of solute at the membrane surface and instead presumed the existence of a completely formed boundary layer. Therefore, the problem of mass transmission was perceived to be limited to only one dimension. The convective-diffusive mass balance, spanning from the surface of the membrane to the film layer, defines the relationship between the flow of permeate and CP, which can be mathematically stated as [10]:

$$\frac{m_{AW}-m_{AP}}{m_{A0}-m_{AP}} = \exp\left(\frac{J}{K}\right) \quad (1)$$

K represents the mass transfer coefficient, m_{A0} represents the bulk solute concentration, m_{AP} represents the permeate solute concentration, and J represents the permeate water flux through the membrane.

The mass transfer coefficient is significantly affected by the flow hydrodynamics, which can be estimated using the empirical correlation [3, 10]:

$$K = \frac{D}{\delta} \tag{2}$$

The solute diffusion coefficient is represented by D, whereas the film layer thickness is denoted by δ.

The correlation between the mass transfer coefficient (k) and the Sherwood number (Sh) can be expressed using the following empirical equation, which was derived specifically for laminar flow[10, 14].

$$Sh = \frac{kd_h}{D} = 1.62\left(\frac{d_h u}{v}\right)^{\frac{1}{3}}\left(\frac{\vartheta}{D}\right)^{\frac{1}{3}}\left(\frac{d_h}{L}\right)^{\frac{1}{3}} \tag{3}$$

The variables in the equation are defined as follows: d_h represents the hydraulic diameter, u represents the flow velocity, ϑ represents the kinematic viscosity, D represents the solute diffusivity in water, and L represents the length of the membrane channel.

The current work postulated that the solution of $MgSO_4$ salt and deionized water exhibited both isothermal and incompressible properties. An examination of the hydrodynamic flow and concentration polarization processes was carried out utilizing the Eulerian-based solution of the continuity, Navier-Stokes, and solute conservation equations.

$$\nabla \cdot \mathbf{u} = 0 \tag{4}$$

While $\mathbf{u} = (u, v)$ is the velocity vector field of the fluid.

Navier–Stokes equation:

$$\frac{\partial \mathbf{u}}{\partial t} + (\mathbf{u} \cdot \nabla)\mathbf{u} = -\frac{1}{\rho}\nabla p + \vartheta \nabla^2 \mathbf{u} \tag{5}$$

The variable p represents the pressure field, and ϑ is the kinematic viscosity.

Mass conservation equation:

$$\frac{\partial c}{\partial t} + u\frac{\partial c}{\partial x} + v\frac{\partial c}{\partial y} = D\left(\frac{\partial^2 c}{\partial x^2} + \frac{\partial^2 c}{\partial y^2}\right) \tag{6}$$

where c is the salt concentration.

The aforementioned differential equations were solved using the following set of boundary conditions:

Feed channel inlet:

$$\begin{aligned} &\mathrm{x} = 0, 0 < \mathrm{y} < \mathrm{h}\ (\mathrm{h} = 3\mathrm{mm}) \\ &u_l = u_{l0}, v_l = 0,\ m_A = m_{A0} \end{aligned} \tag{7}$$

Channel outlet:

$$x = L, 0 < y < h(L = 10cm)$$
$$\frac{\partial u_l}{\partial x} = 0, \frac{\partial v_l}{\partial x} = 0, \frac{\partial m_A}{\partial x} = 0 \quad (8)$$

Upper wall (patterned):

$$0 < x < L, y = h$$
$$u_l = 0, v_l = 0, D\frac{\partial c}{\partial n} = 0 \quad (9)$$

Membrane surface:

$$0 < x < L, y = 0$$
$$v = J_v = L_p\{\Delta P - \sigma[\pi(m_{AW}) - \pi(Rm_{AW})]\}, u = 0 \quad (10)$$

$$D\frac{\partial c}{\partial n} = J_v\left(c_{AW} - c_{Ap}\right) \quad (11)$$

2.3. Mesh independence

The model equations were solved utilizing the specified boundary conditions in COMSOL Multiphysics version 6.1 software. The program employed the finite element method (FEM) to computationally solve the equations. Figure 2 illustrates the generation of an unstructured mesh by the program.

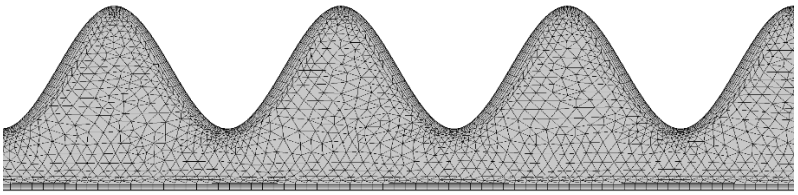

Figure 2. used Mesh quality for sine-wave geometry.

A mesh sensitivity analysis was performed to assure precise outcomes from the model. Given that the permeate flux is influenced by all other system variables, it was employed as a criterion for result comparison and should remain constant regardless of mesh size. Simulation data were analyzed with varying mesh resolutions to determine the ideal element size, ensuring that the impact of the finer mesh does not exceed 1%. A mesh independence study was conducted using a transmembrane pressure of 9 bar, a feed concentration of 2500 mg/l, and a feed flow rate of 2 L/min. Figure 3 illustrates that the maximum permeate flux varies by around 1% while refining the element size from approximately 50K to 75K, but the associated calculation time rises significantly. In this research, an element count of approximately 50K was selected because the variations up to an element count of about 75K were minimal and could be ignored, while the computational cost and time exceeded those associated with an element count of approximately 50K. Consequently, its meshing standard was chosen for subsequent calculations.

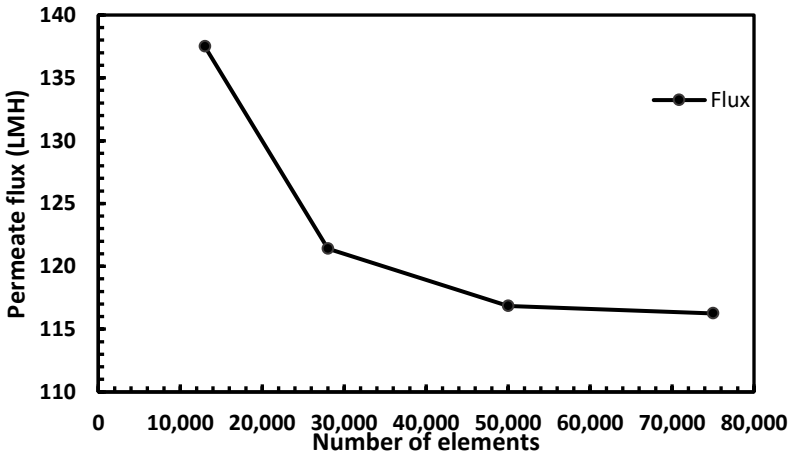

Figure 3. Mesh independence study for Sine-wave geometry (Operating conditions: Q_f = 2L/min; TMP = 9bar; C_f = 2500ppm)

3. Results and Discussion

3.1. Model Validation

The permeate flux was simulated by changing the feed flow rate in a module filled with spacers. The correctness of the model was confirmed by comparing these findings with the relevant data from reference [10]. The results of the model and the experimental data are shown in Figure 4. The results of the simulation and the experiments were quite congruent. The permeate flux may vary by no more than 1.8% across all feed flow rates. This proves that the suggested CFD model is capable of accurately estimating the performance of the nanofiltration system.

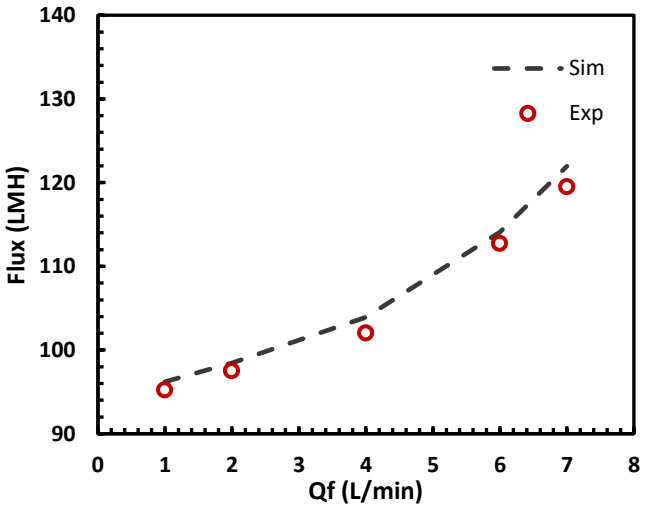

Figure 4. Comparison between experimental (Exp.) and simulation (Sim.) data in a commercial spacer-filled module for permeate flux with feed flow rate (Operating conditions: TMP = 9bar; C_f = 2500ppm)

3.2. Effect of Patterned Walls

Simulations were performed to examine the impact of patterned walls on the permeate flux. To achieve this goal, the simulations were conducted under the assumption of a constant feed concentration of 2500 ppm and a TMP (transmembrane pressure) of 9 bars. Figure 5 exhibits the permeate flux at different feed flow rates and demonstrates that, regardless of the patterns, the permeate flux rises with an increase in the feed flow rate. Given that the fluxes are close to each other at Qf~1 (L/min), it is clear that the form of the pattern does not impact the turbulence of the flow in the feed channel at very low Reynolds numbers.

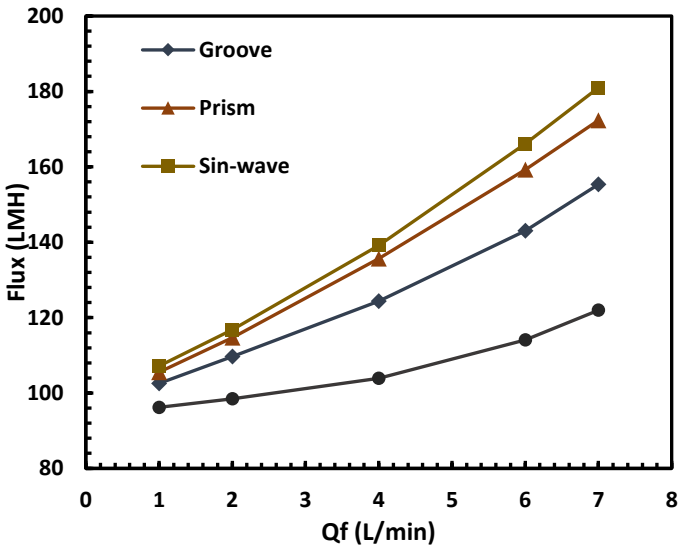

Figure 5. Effect of pattern type and feed flow rate on permeate flux.(Operating conditions: TMP = 9bar; C_f = 2500ppm)

By increasing the Reynolds number, the difference between different patterns becomes more obvious. Between patterned geometries, the groove pattern had the lowest fluxes. Compared to the normal module with a commercial feed spacer [10], the permeate fluxes on the prism and sine-wave patterned plates were respectively 41% and 48% higher. Unlike the prism and sine wave patterns, the groove pattern design has a higher number of inactive areas in the corners of the pattern and achieves a maximum increase in permeate flow of 27%.

Based on the findings of the various geometries, it was determined that the sine-wave patterned channel provided the highest level of performance among the geometries that were investigated. Because of this, it was considered for further investigation.

3.3. RSM Results

The objective of this research is to enhance the efficiency of the nanofiltration system in order to achieve optimal performance, such as maximizing the permeate flux. In order to conduct simulations and analyze data obtained by CFD simulation, the response surface technique with Box-Behnken design mode (RSM-BBD) was used. The Box-Behnken design is favored in CFD studies due to its efficiency and predictive accuracy compared to other response surface methodology designs like Central Composite Design (CCD). BBD requires fewer runs by focusing on mid-level points, which enhances numerical stability and reduces the risk of simulation failures

by avoiding extreme values that can destabilize models. It effectively captures curvature in response surfaces, minimizing overfitting and yielding generalized models. The design of the experiments investigated three primary parameters at three different levels for the sine-wave patterned channel. A total of 13 experiments were analyzed using the RSM-BBD approach. To investigate the optimal conditions for achieving the highest efficiency of the nanofiltration system, we analyzed the feed flow rate, transmembrane pressure (TMP), and feed concentration. The levels of the parameters in the coded mode, together with their corresponding actual contents, are shown in Table 1.

Table 1. The levels of the parameters in the coding mode.

Parameters	Unit	Code	Levels of factors		
			-1	0	1
Q_f	L/min	A	2	4	6
TMP	bar	B	6	9	12
C_f	ppm	C	1000	2500	4000

The simulation results of the permeate flux under the recommended conditions by the RSM-BBD are shown in Table 2. The RSM-BBD developed a second-order model for the permeate flux. Insignificant factors with p-values over 0.1 were eliminated from the original model and the modified model for the permeate flux is presented by Equation 12, which is based on the coded factors.

Table 2. Operating conditions of runs suggested by RSM-BBD.

Run	A: Feed Flow (L/min)	B: TMP (bar)	C: Feed Concentration (mg/L)	Flux (L/m^2h)
1	6	12	2500	248.486
2	4	6	1000	95.0827
3	2	6	2500	70.1978
4	4	12	4000	127.016
5	4	9	2500	139.11
6	6	9	4000	109.881
7	2	9	1000	143.48
8	4	6	4000	61.2207
9	6	9	1000	203.972
10	2	9	4000	77.294
11	2	12	2500	174.793
12	6	6	2500	99.7934
13	4	12	1000	271.476

$$\text{Flux} = 141.49035524066 + 24.545938738077A + 61.934373629423B - 42.324867445C + 11.024348433845AB - 6.97608529AC - 27.64944112BC + 6.2319312103299B^2 - 8.4284828608248C^2 \quad (12)$$

Where $-1 < A.B.C < +1$.

Based on the RSM model, the positive signs of A and B illustrates that the increment of feed flow rate and TMP increases the permeate flux. The negative sign of C indicates that enhancing the salt concentration in the feed flow reduces the permeate flux.

An analysis of variance (ANOVA) was used to examine the accuracy, believability, validity, and significance of the components and model. The findings are shown in Table 3.

Table 3. ANOVA table and statistical information.

Source	Sum of Squares	df	Mean Square	F-value	p-value
Model	54011.94	8	6751.49	341.66	< 0.0001
A-Feed Flow	4820.02	1	4820.02	243.92	< 0.0001
B-TMP	30686.93	1	30686.93	1552.90	< 0.0001
C-Feed Concentration	14331.16	1	14331.16	725.22	< 0.0001
AB	486.15	1	486.15	24.60	0.0077
AC	194.66	1	194.66	9.85	0.0349
BC	3057.97	1	3057.97	154.75	0.0002
B^2	108.74	1	108.74	5.50	0.0789
C^2	198.91	1	198.91	10.07	0.0338
Residual	79.04	4	19.76		
Cor Total	54090.98	12			
R^2	0.9985				
Adjusted R^2	0.9956				
Predicted R^2	0.9831				
%CV	3.17				
Adeq. Precision	56.3755				

The ANOVA analysis of the modified quadratic model (Table 3) demonstrated its statistical significance, with a model p-value of <0.0001, indicating that the independent variables significantly influence the permeate flux. The model's F-value of 341.66 further supports the statistical significance, showing that the variation explained by the model is much greater than the variation due to random error. The R^2 value of 0.9985 suggests an excellent fit, with the model explaining 99.85% of the variability in the response variable. Key factors, including feed flow

rate, TMP, and feed concentration, were found to be highly significant, along with important interactions between these factors. The model also exhibited strong predictive power, as indicated by a predicted R^2 of 0.9831. Overall, the model is robust and suitable for predicting permeate flux in nanofiltration systems, providing valuable insights for optimizing operating conditions.

The residual plots (Figure 6) demonstrated the quality of the established actuarial model. The common eventuality plot (Figure 6a), which depicts the usual residual distribution, is located around the diagonal straight line. Figure 6b shows the residuals plot compared to expected response values. The assumption of permanent variance has been confirmed and accepted. The graph should include a random dispersion. The residual versus simulation run order examines hidden characteristics that may have influenced the response. Keep in mind that the plots in Figure 6b and c should not exceed +3 on the Y-axis.

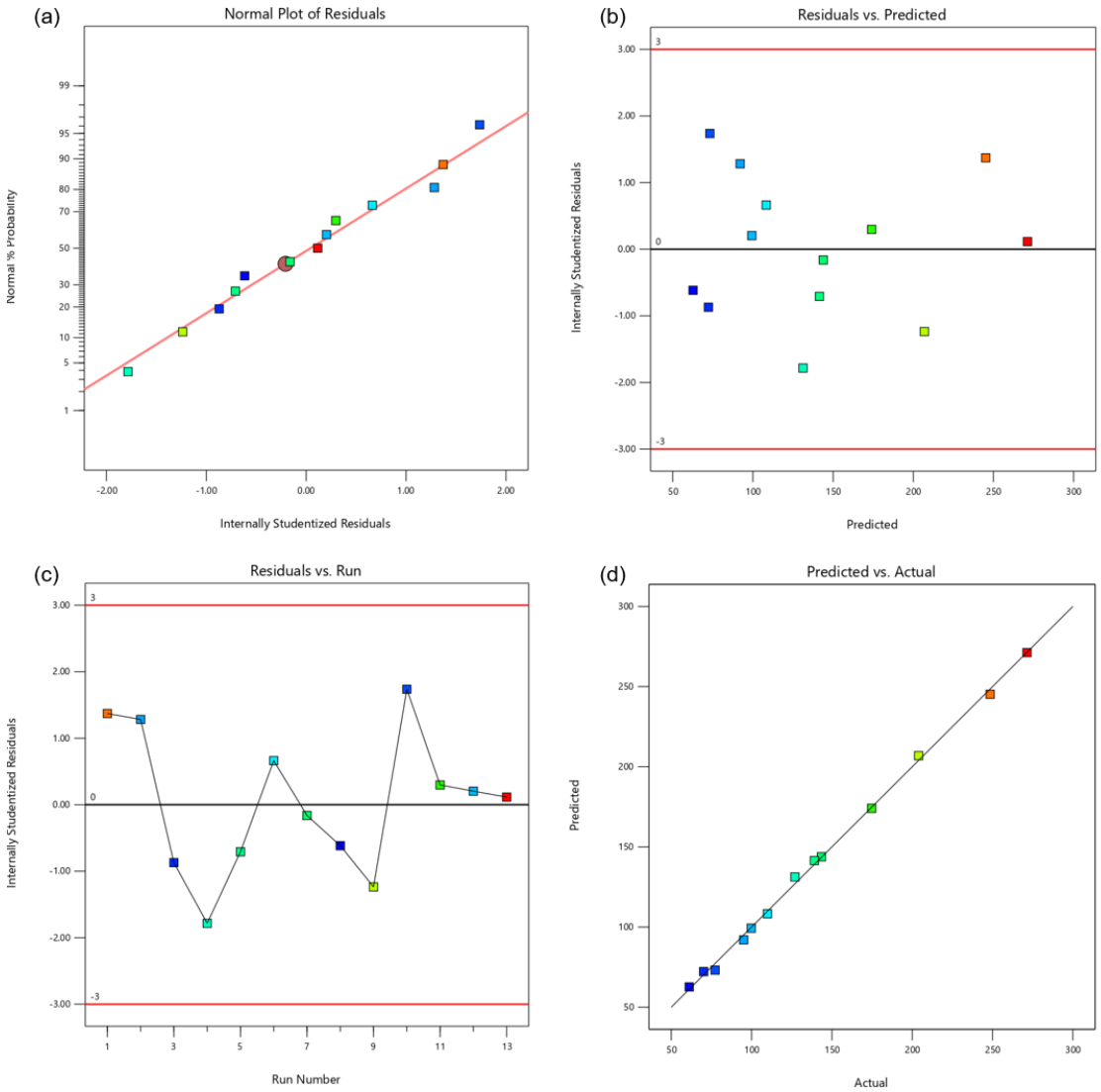

Figure 6. Residual plots and predicted vs. actual plots for RSM-BBD design of the permeate flux.

Figure 6d displays the predicted plot against the values of the actual permeate flux. This helps obtain the value or values that the RSM model is unable to readily prevent. The data points must be split evenly by the 45 diagonal right lines. Figure 6 illustrates that the RSM-BBD model is very consistent with the CFD simulation results. Additionally, the RSM model can be employed to predict the behavior of the nanofiltration system with sine-wave patterned channel.

3.4. Effect of operating parameters

Figure 7 shows 3-D graphs that illustrate how the factors interact with the permeate flow. Figure 7 showed 3D and counter charts illustrating the interactions between the three factors. In both graphs, the third factor is in its middle value. According to Figure 7a and b, the increment of TMP on the permeate flux at different feed flow rates and inlet concentrations has the same trend; that is, the permeate flux is enhanced by increasing the TMP because of the increase in the driving force of the process. Figure 7a illustrates that enhancing Q_f at all TMP values leads to an increase in the permeate flux. This is due to an increase in turbulence and an improvement in mixing in the feed channel, which is achieved by increasing the fluid flow rate and velocity. Figure 7b also demonstrates the impact of variations in feed concentration on the permeate flux. The permeate flux increases by a decrease in the feed concentration at all values of TMP due to decrease in osmotic pressure. This impact is greater at higher values of TMP.

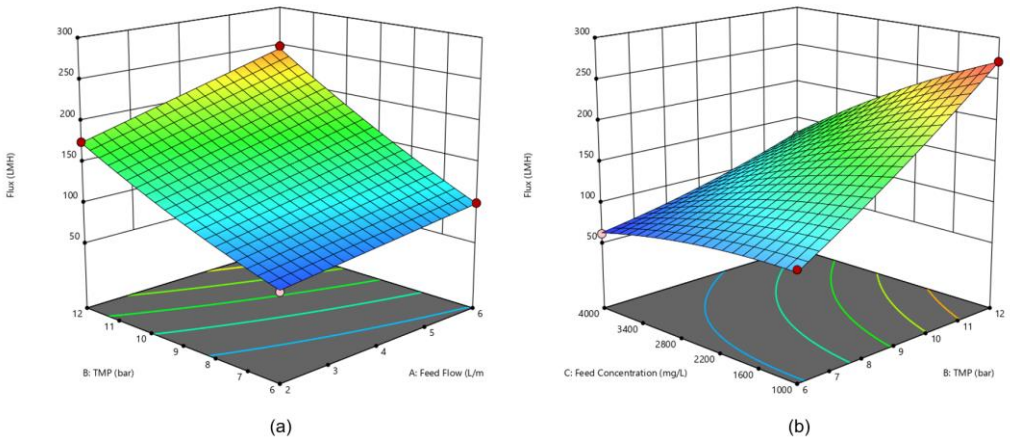

Figure 7. 3D response surfaces for the impact of operating parameters on the permeate flux, a) the flow rate of feed and transmembrane pressure, b) the transmembrane pressure and feed concentration.

3.5. Fluid Hydrodynamics

Fluid hydrodynamics plays a crucial role in nanofiltration module design, as optimizing flow patterns can significantly reduce concentration polarization and fouling. Improved hydrodynamic performance minimizes CP in feed channel, which in turn can lower energy costs by reducing the pressure required to maintain flux and decrease maintenance frequency by reducing fouling-related cleanings. The fluid flow on the surface of the membrane is directly related to the flux and inversely related to the concentration polarization phenomena. This means that increased turbulence leads to less salt accumulation at a specific point. Consequently, the flux increases due to the decrease in osmotic pressure.

In fluid dynamics, "dead zones" refer to areas within the filtration module where water flow is minimal or stagnant. These zones tend to form in corners or around structural components, and

because of the reduced movement, they allow solutes to accumulate on the membrane surface. This buildup intensifies CP, creating a barrier that lowers filtration efficiency and increases the pressure required to maintain flow, thus raising energy costs. Figure 8 demonstrates that the groove pattern exhibits a higher number of dead zones because of having more corners in its geometry. The high number of dead zones in this geometry causes channelization of the flow in the channel and reduces mixing. An increase in CP and solute buildup results from this channelized flow. Because the prism and sine-wave geometries have fewer corners, they exhibit fewer dead zones and provide effective mixing inside the channel, which reduces concentration polarization and enhances flux.

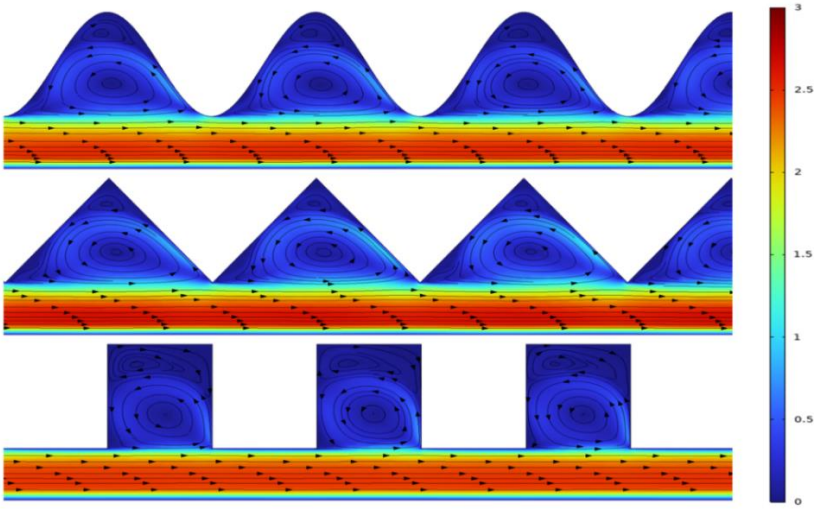

Figure 8. Development of mixture velocity in patterned feed channels (m/s).

4. Conclusion

This study utilized a 2D CFD simulation to examine the enhancement of flux in nanofiltration of an aqueous solution of $MgSO_4$ using a membrane module with patterned channel (sine-wave, prism, groove patterns). The COMSOL Multiphysics program was used to solve basic transport equations of momentum and mass transfers in the model domains using the finite element method. The experimental data perfectly confirmed the model's results. The impact of different pattern types and feed flow rates on the permeate flux was investigated. The findings revealed that the use of patterned walls had a significant effect on the permeate flux. Among the patterns studied, the sine-wave and prism-patterned walls exhibited a greater increase in permeate flux compared to the groove pattern. However, the groove-patterned channel still had a notable impact on the permeate flux in comparison to regular modules with commercial feed spacer, despite having the lowest flux among the patterned geometries.

Considering that the sine-wave pattern performed the best among the investigated geometries, with a maximum increase of 48% of the permeate flux. The effect of different operating parameters on permeate flux in a nanofiltration module with a Sine-wave patterned channel was studied using response surface methodology (RSM). According to RSM results, increasing the feed flow rate or transmembrane pressure (TMP) significantly increased the permeate flux. On the other hand, the permeate flux decreased as feed concentration increased.

The main focus of this research was on examining the geometry of the patterns in the channel, and the periodic length of all of them was considered to be 2.78 mm. In order to investigate more

deeply the effect of creating geometric patterns in the feed channel, in future researches, it is possible to obtain the optimal periodic length by changing this parameter for each geometry. Also, the experimental study of creating these geometric patterns in the feed channel can be an important step towards better understanding the effect of creating these patterns in the feed channel and confirming the validity of the data obtained in this research.

Nomenclature

c	salt concentration (kg/m³)
d_h	hydraulic diameter (m)
D	diffusion coefficient (m²/s)
g	gravitational force (m/s²)
h	channel height (m)
J_v	permeate volume flux (m/s)
k	mass transfer coefficient (m/s)
L	membrane channel length (m)
L_P	hydraulic conductivity (m²/(Pa·s))
M	interfacial momentum source term (kg/m²s²)
m_A	solute mass fraction (kg solute/kg solution)
m_{Aw}	solute mass fraction on membrane surface (kg solute/kg solution)
p	pressure (Pa)
R	true rejection
TMP	transmembrane pressure (Pa)
u	velocity in x-direction (m/s)
v	velocity in y-direction (m/s)

Greek letters

δ	film layer thickness (m)
μ	viscosity (kg/m·s)
ϑ	kinematic viscosity (m²/s)
π	osmotic pressure (Pa)
ρ	density (kg/m³)

Subscripts

l	liquid phase
P	permeate side
w	solution adjacent to the wall
0	bulk solution

References

1. Abadikhah H, Zokaee Ashtiani F, Fouladitajar A (2015) Nanofiltration of oily wastewater containing salt; experimental studies and optimization using response surface methodology. Desalination Water Treat 56:2783–2796. https://doi.org/10.1080/19443994.2014.966331
2. Zeng K, Zhou J, Cui Z, Zhou Y, Shi C, Wang X, Zhou L, Ding X, Wang Z, Drioli E (2018) Insight into fouling behavior of poly(vinylidene fluoride) (PVDF) hollow fiber membranes

caused by dextran with different pore size distributions. Chin J Chem Eng 26:268–277. https://doi.org/10.1016/j.cjche.2017.04.008
3. Mulder M (1991) VI MEMBRANE PROCESSES. In: basic principles of membrane technology
4. Geraldes V, Afonso MD (2007) Prediction of the concentration polarization in the nanofiltration/reverse osmosis of dilute multi-ionic solutions. J Memb Sci 300:20–27. https://doi.org/10.1016/j.memsci.2007.04.025
5. Prabhavathy C, De S (2010) Estimation of transport parameters during ultrafiltration of pickling effluent from a tannery. Sep Sci Technol 45:11–20. https://doi.org/10.1080/01496390903401788
6. Subramani A, Kim S, Hoek EMV (2006) Pressure, flow, and concentration profiles in open and spacer-filled membrane channels. J Memb Sci 277:7–17. https://doi.org/10.1016/J.MEMSCI.2005.10.021
7. Ahmad AL, Lau KK (2006) Impact of different spacer filaments geometries on 2D unsteady hydrodynamics and concentration polarization in spiral wound membrane channel. J Memb Sci 286:77–92. https://doi.org/10.1016/J.MEMSCI.2006.09.018
8. Sreedhar N, Thomas N, Al-Ketan O, Rowshan R, Hernandez H, Abu Al-Rub RK, Arafat HA (2018) 3D printed feed spacers based on triply periodic minimal surfaces for flux enhancement and biofouling mitigation in RO and UF. Desalination 425:12–21. https://doi.org/10.1016/J.DESAL.2017.10.010
9. Monfared MA, Kasiri N, Salahi A, Mohammadi T (2012) CFD simulation of baffles arrangement for gelatin-water ultrafiltration in rectangular channel. Desalination 284:288–296. https://doi.org/10.1016/J.DESAL.2011.09.014
10. Asefi H, Alighardashi A, Fazeli M, Fouladitajar A, Asefi H, Alighardashi A, Fazeli M, Fouladitajar A (2020) Investigation of concentration polarization in a cross-flow nanofiltration membrane: Experiment and CFD modelling. JOURNAL OF HYDRAULIC STRUCTURES Shahid Chamran University of Ahvaz Journal of Hydraulic Structures J Hydraul Struct 6:1–19. https://doi.org/10.22055/jhs.2020.31418.1124
11. Fadhila H, Stafford J, Davies PA (2024) Direct numerical simulation of flow in a membrane channel under oscillating inlet conditions. Desalination 590:117950. https://doi.org/10.1016/J.DESAL.2024.117950
12. Dun RK, Wang YL, Liu BZ, Shen H, Wang DS, Jia WJ, Nie RF (2024) Study on the nanofiltration membrane fouling control and cleaning efficiency of micro- and nanobubbles. Desalination Water Treat 317:100297. https://doi.org/10.1016/J.DWT.2024.100297
13. Shang W, Li X, Liu W, Yue S, Li M, von Eiff D, Sun F, An AK (2021) Effective suppression of concentration polarization by nanofiltration membrane surface pattern manipulation: Numerical modeling based on LIF visualization. J Memb Sci 622:119021. https://doi.org/10.1016/J.MEMSCI.2020.119021
14. Li QY, Ghosh R, Bellara SR, Cui ZF, Pepper DS (1998) Enhancement of ultrafiltration by gas sparging with flat sheet membrane modules. Sep Purif Technol 14:79–83. https://doi.org/10.1016/S1383-5866(98)00062-8.